Artificial Intelligence Techniques for Controlling PV- Wind Powered Rural Zone in Egypt

H. M. Fargli[1], F. H. Fahmy[1], and M.A. H.EL-Sayed[2]

[1]Electronics Research Institute
National Research Center Building
Cairo, Egypt
Phone number:+202 33310512, e-mail: farghally555 @yahoo.com

[2]Center of Energy Studies, University of Trinidad and Tobago

Abstract. In remote areas, electricity could still be available if stand-alone renewable electricity power sources are used . One of the most promising applications of renewable energy technology is the installation of hybrid energy systems, where the cost of grid extension is prohibitive and the price of fuel increases drastically with the remoteness of the location. It has been demonstrated that hybrid energy systems can significantly reduce the total life cycle cost of stand-alone power supply, while at the same time providing a more reliable supply of electricity .Due to the high nonlinearity characterizing the PV-Wind hybrid system it would be impractical to develop rigorous mathematical model and at the same time obtain a simple and effective controller.

In this paper, a control system, which includes either the Neural Network Controller (NNC) or the Fuzzy Logic. Controller (FLC) controller is developed for achieving the coordination between the components of a PV-Wind hybrid system as well as control the energy flows. The performance of the system is evaluated by comparing the performance of the system using the NNC and the FLC. Also, this work presents a complete mathematical modeling and MATLAB simulink model for the different components of the hybrid system.

Key words

Hybrid system, photovoltaic system, wind system, battery bank.

Neural controller, fuzzy logic controller.

1. Introduction

Due to intermittent natural energy resources and energy resources seasonal unbalance, a PV-wind hybrid electrical power supply system was developed for many remote locations where a conventional grid connection is inconvenient or expensive [1]. .Due to the high nonlinearity characterizing the PV-Wind hybrid system it would be impractical to develop rigorous mathematical model and at the same time obtain a simple and effective controller

Artificial intelligence (AI) techniques are becoming useful as alternate approaches to conventional techniques or as components of integrated systems. They have been used to solve complicated practical problems in various areas and are becoming more and more popular nowadays. AI-techniques have the following features: can learn from examples; are fault tolerant in the sense that they are able to handle noisy and incomplete data; are able to deal with non-linear problems; and once trained can perform prediction and generalization at high speed. AI-based systems are being developed and deployed worldwide in a myriad of applications, mainly because of their symbolic reasoning, flexibility and explanation capabilities. AI have been used and applied in different sectors, such as engineering, economics, medicine, military, marine, etc. They have also been applied for modeling, identification, optimization, prediction, forecasting, and control of complex systems .

Nowadays, considerable attention has been focused on use of artificial neural network (ANN) on system modeling and control applications. Neural networks, with their remarkable ability to derive meaning from complicated or imprecise data, can be used to extract patterns and detect trends which are too complex to be noticed by either humans or other computer techniques. A trained neural network can be thought of as an "expert" in the category of information it has been given to analyze. The ANN has several key features include Adaptive learning and Self-Organization .Also NNs are characterized by the rapidity of response and robustness, which make them attractive to control [2].

Recently the concept of fuzzy logic control (FLC) has been employed in many industrial applications. The use of FLC significantly changes the control approach compared with that of conventional control approaches. A conventional controller adjusts the system control parameters on the basis of an accurate mathematical model of the process dynamics. In the case of a fuzzy

rules-based expert system, it is a logical model of the human behavior of the process operator (linguistic information). Also FLC usually leads to better results than those of the conventional controllers, in terms of response time, settling time and robustness [3].

The emphasis of this paper is concerned with the control of the energy flow of PV-Wind hybrid system using either the NN or the FL techniques. The PV-Wind hybrid system is applicable in three buildings (i.e. school, home & emergency hospital) in a remote area in the Eastern Desert for supplying the required electrical loads. Also, a complete mathematical modeling and MATLAB simulink model for the different components of the hybrid system is presented in this paper.

2. System Description and Modeling

The block diagram of the system adopted in this paper is shown in Fig. 1. It consists of a PV generator, battery bank and wind turbine. An overall power management controller is designed for the system to coordinate the power flows among the different energy sources.
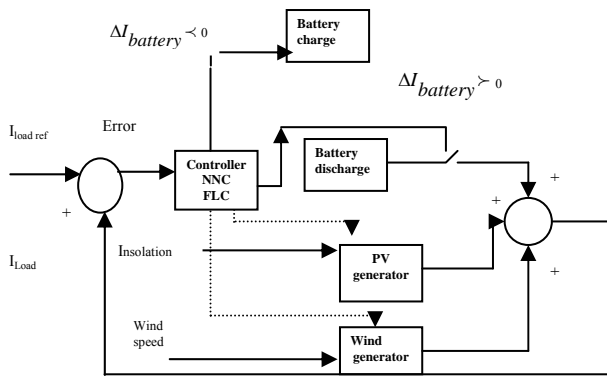

Fig. 1 Proposed Control system of the hybrid PW/wind system

A. The Photovoltaic Array Model

The output current of the PV array consisting of several PV modules can be expressed as [4]:

$$I_{PV} = MI_l - MI_0\left[\exp\left(\frac{q\left(NV_{PV} + \frac{I_{PV}R_S N}{M}\right)}{NAKT_C}\right) - 1\right]\left[\frac{NV_{PV} + \frac{I_{PV}R_S N}{M}}{\frac{NR_{Sh}}{M}}\right] \quad (1)$$

Where I_{PV}: output current of panel (A), I_l : light generated current per module (A),
I_o: reverse saturation current per module (A), M: number of module strings in parallel, N : number of modules in each series string, V_{PV} terminal voltage for module (V), Rs: diode series resistance per module (ohms), Rsh :diode shunt resistance per module (ohms), q : electric charge ($1.6 \cdot 10^{-19}$ C), k : the Boltzmann constant ($1.38 \cdot 10^{-23}$ J/K), A : diode ideality factor for the module, and T_C :cell temperature (K).

I_{PV} depends on the incident irradiance on the module and the cell operating temperature.

I_o is basically a function of cell temperature only. T_C is affected by external factors such as global irradiance, ambient temperature and wind speed. R_s, R_{sh} and A are constant values for a particular PV module. A PV module manufacturer can provide the necessary information, which needs to be used to estimate most of the parameters in the above equation.

From the above equation, under the short-circuit condition, the panel output voltage
is zero, and the panel output current is a maximum and is called the short-circuit current, I_{sc}. In this condition, the light-generated current becomes equal to the short circuit current since R_s is very small unless the light is concentrated.

This model expresses Isc as a function of solar irradiance and temperature.

$$I_l = I_{SC} = P_1 G\left[1 - P_2\left(G - G_r\right) + p_3\left(T_C - T_r\right)\right] \quad (2)$$

Where P_1, P_2, P_3:constant coefficients for I_{sc}, G_r :reference solar irradiance (W/m2),
G: solar irradiance (W/m2), and T_r:reference temperature (K)..

Normally, 1000 W/m2 and 298 K are selected as the reference solar irradiance and reference temperature, respectively

The reverse saturation current is a small current flowing back through the PV arrays all the time. To estimate this current, an exponential expression which is a function of cell temperature is used

$$I_0 = BT_C^3\left[\exp\left(-\frac{Eg_0}{KT_C}\right)\right] \quad (3)$$

where Eg_o :band gap energy at 0 K (1.16 eV for silicon) and B :a material constant which has to be estimated by using both the manufacturer's data and the I-V curve characteristic of PV module.

The PV cell temperature, T_C, is a parameter that affects the PV output current. To solve for T_C, a thermodynamic analytical model is used based on the overall energy balance of the photovoltaic panel. The absorbed solar energy is converted into electrical energy output, thermal radiative and convective energy losses, and thermal energy stored in the PV module, causing the change in T_C. The rate of change of T_C is suggested by

$$\left(mC_{P \, module}\right)\frac{dT_C}{dt} = Q_{in} - Q_{conv} - Q_{elect} \quad (4)$$

Where $mC_{pmodule}$: effective thermal capacity of the PV module (J/K) at temperature T_C, Q_{in} : solar energy absorbed by the module (W), Q_{rad} :radiative heat loss (W), Q_{conv} : convective heat loss (W) and Q_{elect} : electrical power produced (W).

The solar energy absorbed by the photovoltaic module is expressed as:

$$Q_{in} = \alpha_{abs} GS_P \quad (5)$$

Where α_{abs} : overall absorption coefficient, Sp: total area

of PV module (m^2) and G: global solar radiation on the PV module surface (W/m^2).

The energy loss due to convection is given by the expression below:

$$Q_{conv} = S_P H (T_C - T_a) \qquad (6)$$

Where H: the convective heat transfer coefficient. and is expressed as :

$$H = 1.2475 [\Delta T \cos \beta]^{\frac{1}{3}} + 2.685 u \qquad (7)$$

Where ΔT: normal temperature difference (T_C–T_a), β : tilt angle (degrees) and u wind speed (m/s).

The last parameter, electrical power produced, is expressed as:

$$Q_{elect} = \eta G S_C \qquad (8)$$

Where η: module instantaneous efficiency and S_C: total surface area of PV cells in a module receiving solar radiation.

It is noted that the power output of a PV cell drops as cell temperature increases.

The instantaneous efficiency is therefore a function of the temperature of the module of the PV cell; that is:

$$\eta = \eta_o [1 - \gamma (T_C - T_r)] \qquad (9)$$

Where Tr: reference temperature (298 K), η_O : module efficiency at reference temperature and γ :coefficient for photovoltaic conversion efficiency. The values of γ and η_o are normally obtained from the PV characteristic curves given in the manufacturer's specification sheet .Table 1 summarizes all parameters of the PV panel.

Table 1 PV module coefficients used in the PV array model

Coefficient	Values
Diode factor(A)	38.59
Series resistance (Rs)	2.58 ohm
Shunt rssistance (Rsh)	250 ohm
Total surface area of the PV module (S_P)	0.617 m^2
Total surface area of cells in module (S_c)	0.5625 m^2
Coefficients of I_{SC}	
P1 P2 P3	$4.1*10^{-3}$ m^2/V $-3.73*10^{-4}$ m^2/W $-2.44*10^{-3} K^{-1}$
Coefficient of I_0 (B)	7100 A/K^3
module efficiency at reference	12%
effective thermal capacity of the PV module (m$C_{p\ module}$)	9250 J/K
Temperature coefficient (γ)	0.0045 K^{-1}
Overall absorption coefficient (α_{abs})	0.73

B. Battery Modeling

The following equations are derived empirically from the manufacturer's data [5]

1. Discharge voltage modeling

The current and voltage during discharge case can be described in terms of the soc of the cell (ranging from 0 to 1.0) by

$$V_{bd} = V_r - \frac{I}{AH} \left(\frac{0.189}{soc} + R_i \right) \qquad (10)$$

Where soc is the ratio of the charge at the time of interest to the maximum charge. The other symbols are defined as follows:

$$V_r = 2.094 [1.0 - 0.001 (T - 25\,°C)] \qquad (11)$$

Where
V_r is the rest voltage (V)
V is the terminal voltage(V)
I is the current (A)
AH is the ampere-hour rating of the battery for the discharge rate,

$$R_i = 0.15 [1.0 - 0.02 (T_{air} - 25°C)] \qquad (12)$$

is the internal resistance of the cell (Ω)

T_{air} is the ambient temperature(^{o}C).
The factor of 0.189 represents the internal resistance due to polarization.

2. Charge Voltage Modeling

During the charging period, the current-voltage relationship is given by

$$V_{bc} = V_r + \frac{I \left[0.189 \Big/ (1.142 - soc) + R_i \right]}{AH} + (soc - 0.9) \ln \left(300 \frac{I}{AH} + 1.0 \right) \qquad (13)$$

C. Wind Energy Conversion System

The power extraction of wind turbine is a function of three main factors: the wind power available, the power curve of the machine and the ability of the machine to respond to wind fluctuation. The expression for power produced by the wind is given by [6-8]

$$p_m(u) = \frac{1}{2} C_p (\lambda, \beta) \rho \pi R^2 u^3 \qquad (14)$$

Where ρ is air density, R is radius of rotor, u is wind speed, C_p denotes power coefficient of wind turbine, λ is the tip-speed ratio and β represents pitch angle.

The tip speed ratio is defined as

$$\lambda = \frac{R \omega}{u} \qquad (15)$$

Where u is the rotor speed. It is seen that if the rotor speed is kept constant, then any change in the wind speed will change the tip-speed ratio, leading to the change of power coefficient C_p as well as the generated power out of the wind turbine. If, however, the rotor speed is adjusted according to the wind speed variation, then the tip-speed ratio can be maintained at an optimal point, which could yield maximum power output from the system.

From Eqs. (14) and (15) we can see that

$$P_m(\omega) = k_w \omega^3 \qquad (16)$$

Where

$$k_w = \frac{1}{2} C_p \rho\pi \frac{R^5}{\lambda^3} \qquad (17)$$

For a typical wind power generation system, the following simplified block diagram (Fig. 2) is used to illustrate the fundamental work principle. We see that such a system primarily consists of an aero turbine, which converts wind energy into mechanical energy, a gearbox, which serves to increase the speed and decrease the torque and a generator to convert mechanical energy into electrical energy.
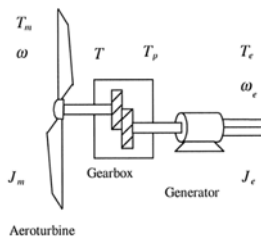
Fig. 2 Schematic diagram of wind power system.

Driving by the input wind torque T_m., the rotor of the wind turbine runs at the speed ω. The transmission output torque T_P is then fed to the generator, which produces a shaft torque of T_e at generator angular velocity of. ω_e .Note that the rotor speed and generator speed are not the same in general, due to the use of the gearbox. The dynamics of the system can be characterized by the following equations:

$$T_m - T = J_m \dot{\omega} + B_m \omega + K_m \theta \qquad (18)$$

$$T_p - T_e = J_e \dot{\omega}_e B_e \omega_e + K_e \theta_e \qquad (19)$$

$$T_p \omega_e = T\omega \qquad (20)$$

where B_m , K_m, B_e, K_e are the friction- and torsion-related constants , T_m, T_e , T, T_P the shaft torque seen at turbine end, generator end, before and after gear box, J_m, J_e the moment of inertia of the turbine and the generator, and ω, ω_e the angular velocity of the shaft at turbine end and generator end.
the gear ratio γ is defined as

$$\gamma = \frac{\omega_e}{\omega} \qquad (21)$$

Upon using Eqs. (19) and (20), we can combine Eqs. (17) and (18) to get

$$J\dot{\omega} + B\omega + K\theta = T_m - \gamma T_e \qquad (22)$$

or equivalently

$$J\dot{\omega} + B\omega + K\theta = \frac{P_m}{\omega} - \gamma \frac{P_e}{\varpi_e} \qquad (23)$$

With

$$J = J_m + \gamma^2 J_e \qquad (24)$$

$$B = B_m + \gamma^2 B_e \qquad (25)$$

$$K = K_m + \gamma^2 K_e \qquad (26)$$

Where P_m denotes the wind power given by Eq. (3) and P_e represents the electric power generated by the system. It is well known that P_e is related to the excitation current of the generator via

$$P_e = K_\phi \omega_e c(I_f) \qquad (27)$$

Where K_ϕ is a machine-related constant, $c(I_f)$ is the flux in the generating system, and I_f is the field current. The exciter dynamics of the system is governed by

$$L\dot{i}_f + I_f R_f = v_f \qquad (28)$$

Where , L is the inductance of the circuit, I_f the field current, R_f the resistance of the rotor field, and v_f the field voltage.

3. Control strategy

During this operation of the hybrid PV/wind system, different situations may appear:
1.The total current generated by the PV and Wind generators is greater than the current needed by the load. In this case, the energy surplus is stored in the batteries and the controller puts the battery in charge condition .When the battery soc reaches a maximum value, the control system stops the charging process.
2. The total PV and wind generators current is less than the current needed by the load, the energy deficit is covered by the storage and the controller puts the battery in the discharge condition. if the battery capacity decreases to their minimum level, socmin, the control system disconnects the load and the energy deficit
3..In case of inverter input and total power equality, the storage capacity remains unchanged.
The NN controller is designed to give three outputs; these are as given the controller output current $\Delta I_{battery}$, the PV Array switching , the wind turbine switching.
 It is cleared that the used PV is able to generate electricity, whenever there is solar illumination; where the electric power is proportional to the incident insolation level. The wind turbine begins to produce output when the wind speed is greater than the cut-in speed until furling speed v_f is reached, at which point the machine shuts down. Off line training for the proposed NNC was applied. Data for off-line training can be obtained either by simulation or experiment. The network is trained to recognize the relationships between the input and output parameters. The BP algorithm uses the supervised training technique. In this technique, the interlayer connection weights and the processing elements' thresholds are first initialized to small random values. The network is then presented with a set of training patterns, each consisting of an example of the problem to be solved (the input) and the desired solution to this problem (the output). These training patterns are presented repeatedly to the ANN model and the adjustment is performed after each iteration whenever the network's computed output is different from the desired output. This process continues until weights converge to the desired error level or the output reaches an acceptable level. For this present work, the data is obtained by

simulating the proposed system. After many trials, the developed NNC, shown in Fig. 3 eventually employed a 4-neuron input, an 8-neuron hidden layer, and 3-neuron output layer. The input network parameters are; the reference load and the difference between the output generation, the reference load, the wind speed and the solar insolation

The inputs to the FLC are: the error signal (e), indicating the difference between the output generation and the reference load and the derivative of this error signal (Δe). The output of the FLC is the controller output current $\Delta I_{battery}$.

Standard triangular membership functions, as shown in Fig. 4 , are chosen for both the inputs and output of the fuzzy logic controller. The fuzzy rule table of these sets is given in Table 2.

Fig. 3 NNC structure.

$\mu(e)$, $\mu(\Delta e)$, or $\mu(\Delta I_{battery})$

e, Δe, or $\Delta I_{battery}$
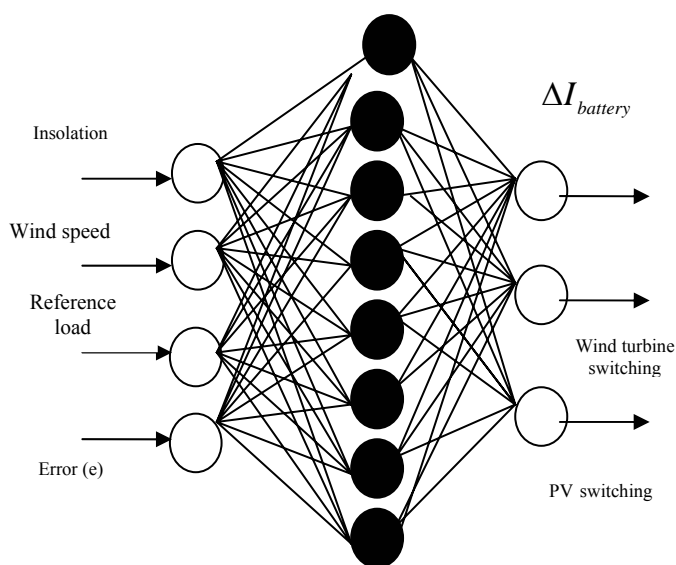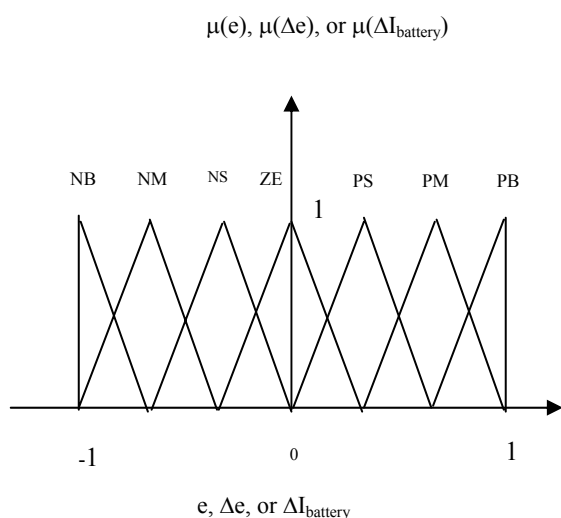
Fig. 4. Membership functions of the fuzzy sets.

4. Matlab Simulation of the Proposed System

In this section, models of the basic components of suggested hybrid system are simulated using Matlab Software [9]. These are the PV array, the wind turbine and the battery storage subsystems. A control system, which includes either the NNC or the FLC controller is developed for achieving the coordination between the components of a PV-Wind hybrid system as well as control the energy flows. The simulation models with both NNC and FLC are shown in Figs 5 & 6 respectively. As cleared, both the two models are driven by forcing functions, such as load profiles and meteorological data (solar radiation,wind speed and temperature data).

The inputs to The PV subsystem are insolation, the wind speed and temperature variables. While, the outputs are the PV current and power.

In the 'wind turbine' subsystem shown in the simulation models , the wind speed is taken as input and the power curve data are used to determine the dynamic magnitude of the captured wind power.

The battery component as shown has two inputs which are the current and the ambient temperature. The output voltage V_{BC} and V_{BD} are the battery voltage during charge and discharge respectively. The presented model does not include the effects of battery self discharge and battery aging. Battery aging refers to the number of charge- discharge cycles the battery has undergone. Self-discharge can be neglected in PV applications where the battery is continuously operated. The capacity loss due to self-discharge is equalized frequently by charging the battery with PV energy.

As shown in Fig. 5 , the NN controller is designed to give three outputs; these are as given the controller output current $\Delta I_{battery}$, the PV Array switching , the wind turbine switching. The training and test cases have been calculated with the help of NN tool box. The training data have been processed with Back-Propagation, BP, learning algorithm to compute the weights for the network architectures under study .For the present work, such NNC structure gave satisfactory results with small number of neurons, hence better in terms of memory and time required to implement the NN in control. The transfer function used in the hidden layer is the "sigmoid", while "purellin" transfer function is used for the output layer. The training process has been carried out over 1000 epochs.

The proposed controller in Fig. 6 is a two-input single-output FLC. The controller inputs are the error e and the change of error Δe at the current sampling interval k, while the controller output is the change in control current $\Delta I_{battery}$.

5. Simulation results

In this section the results of the the PV/ Wind hybrid System are reported. As discussed before, the system is designed to supply electric power for three different buildings (school, hospital and home).

Table 6.2 The rule table of the designed FLC

e \ Δe	NB	NM	NS	ZE	PS	PM	PB
NB	NB	NB	NB	NB	NM	NS	ZE
NM	NB	NB	NB	NM	NS	ZE	PS
NS	NB	NB	NM	NS	ZE	PS	PM
ZE	NB	NM	NS	ZE	PS	PM	PB
PS	NM	NS	ZE	PS	PM	PB	PB
PM	NS	ZE	PS	PM	PB	PB	PB
PB	ZE	PS	PM	PB	PB	PB	PB
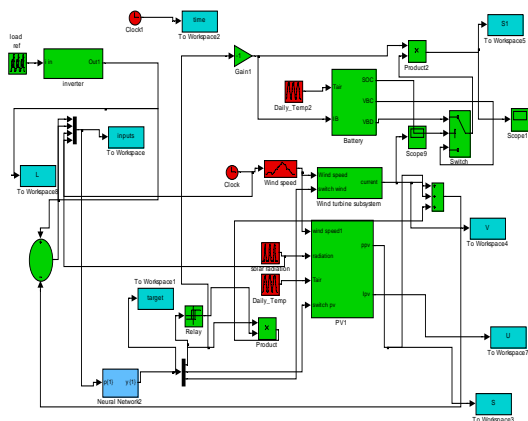
Fig. 5 The simulink block diagram of the electrical system with NNC.
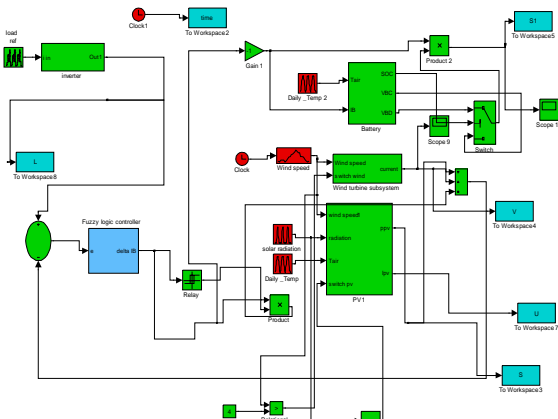
Fig.6 The simulink block diagram of the electrical system with FLC.

Fig. 7 shows the real daily variation of the solar insolation profile. The corrected real daily wind speed profile and air temperature on the day the data were collected are shown in Figs. 8 & 9. The output power from the PV array in the system over the 24 hour simulation period is shown in Fig. 10. The variations of PV output have the same tendency as the solar insolation. The temperature plays an important role in the PV cell's performance. The PV cell temperature is estimated by the PV thermal model. Fig. 11 shows the PV temperature response over the simulation period. Two main factors for determining the PV cell temperature are the solar insolation and the air temperature (surrounding temperature) as shown in figure.

It is noted from Fig. 11 that the PV cells cool down to about the same surrounding air temperature at sunset. The cell temperature climbs up in case of sunrise.

The output generation from the wind energy conversion unit in the hybrid energy system over the 24 hour simulation period is shown in Fig.12. The plot for the battery power and the battery state of charge are shown in Fig. 13&14 respectively.
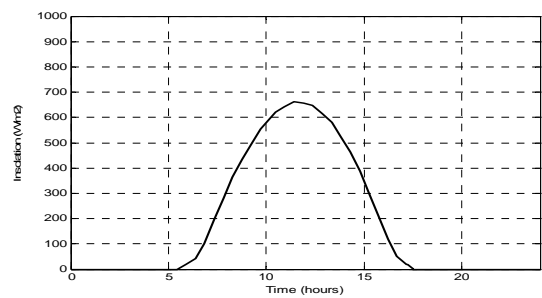

Fig. 7 Actual daily solar insolation profile .
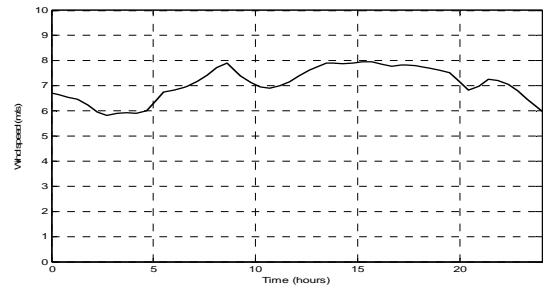

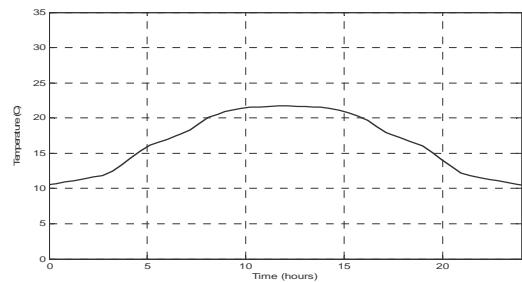Fig. 8 Actual daily wind speed profile .

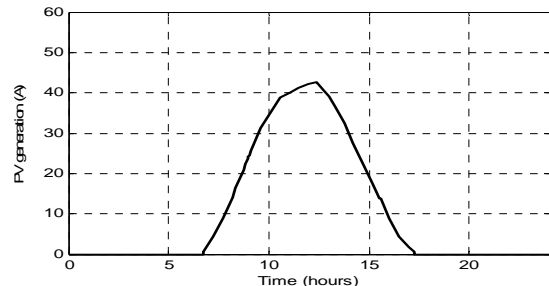Fig. 9 Actual daily   ambient temperature profile

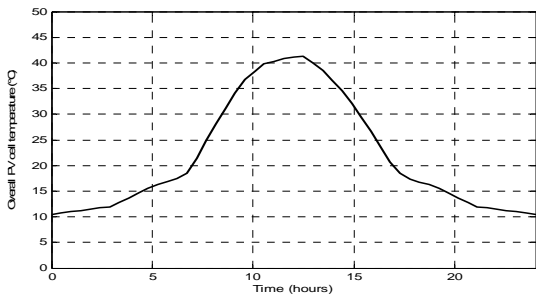Fig.10 PV generator current over the simulation period.

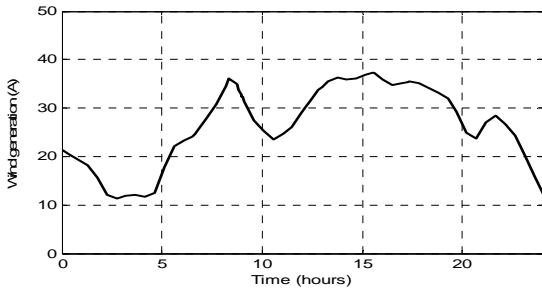Fig. 11 The PV temperature response over the simulation period

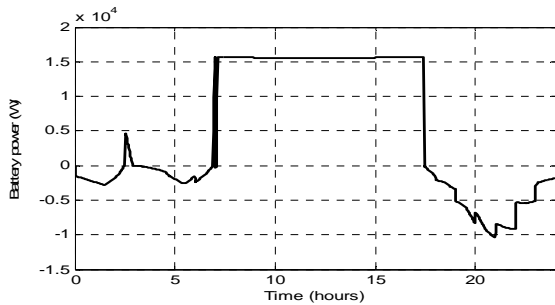Fig. 12 Wind generator power over the simulation period
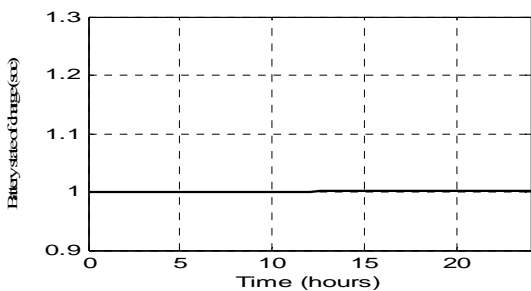

Figur13 The battery power over the simulation period

Fig. 14 The lead acid battery state of charge versus time.

A. NNC Results

One of the important aspects of applying a NN to any particular

problem is to formulate the inputs and outputs of the NN structure under study. Off line training for the proposed NNC was applied. Data for off-line training can be obtained either by simulation or experiment. For this present work, the data is obtained by simulating the proposed system in an open-loop system. The simulation is carried out for different values of wind speeds, solar insolation and ambient temperature along one day

Fig. 15 shows the NNC outputs through 24 hours on the day the data were collected. These are, as given, the controller output current $\Delta I_{battery}$, the PV Array switching, the wind turbine switching. It is cleared that the used PV is able to generate electricity, whenever there is solar illumination; as the electric power is proportional to the incident insolation level. The NNC switch PV on in the morning when sufficient solar radiation is available. While it is switched off in the evening after sunset. The wind turbine begins to produce output when the wind speed is greater than the cut-in speed until furling speed V_F is reached, at which point the machine shuts down. So the switching signal of the wind turbine exists whenever the wind speed is in that range.
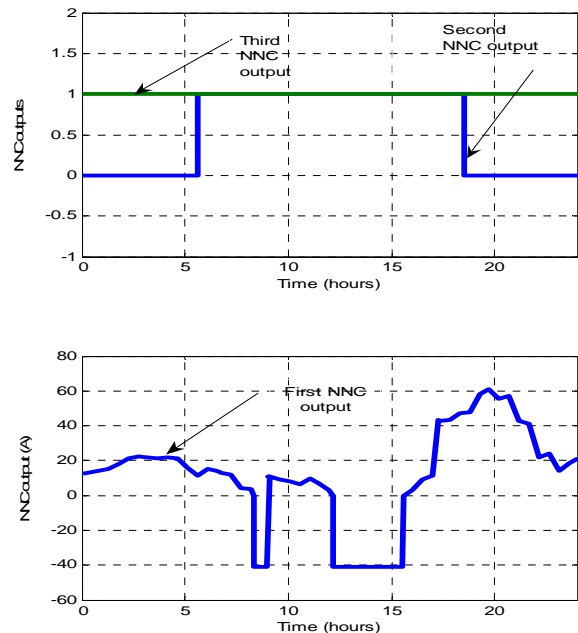

Fig. 15 NNC outputs

B. FLC Results

The main object of the FLC is to cover the load which is achieved by adjust the battery power when the output generation from the photovoltaic cells and wind turbines is not enough. Also, it allows charging the battery from the photovoltaic cells and winding turbines power when the generating power exceeds the load power.

There are three parameters, used as scaling factors for the FLC design, two input parameters K_e, and $K_{\Delta e}$ and one output parameter $K_{\Delta u}$. These parameters are adjusted, using the knowledge about the nature of e, Δe, and Δu and also by using trial and error, until best performance is achieved. The Scaling factors are set as follows Ke= 0.01 , $K_{\Delta e}$ = 0.02 , and KΔu =2

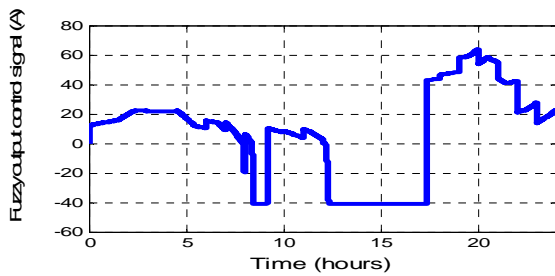Fig. 16 illustrates the resulting controller output over 24 hours.

Fig. 16 Fuzzy controller output

C.   The Best Controller

Fig.17 illustrates a comparison between the responses of control output generation under the effect of several insolation levels, wind speed through 24 hours using either the FLC or the NNC controller. Also this figure shows the reference load, which is the total electrical load of the three buildings. It is clear that the FLC has a better response than NNC. The error between the generation and load resulting with NNC &FLC is shown in Figs. 18 &19 respectively. It is cleared that the error resulting with FLC approximately zero during the whole day. While the error resulting with NNC is reaching zero at most time except the period (12 p.m. to 3 p.m.). This indicates the more accuracy of FLC than NNC.
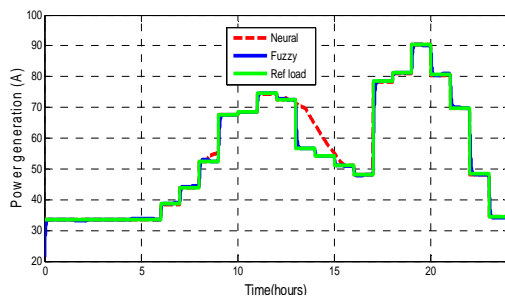

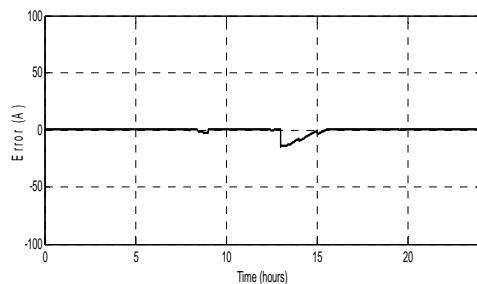Fig. 17 current generating with NNC and FLC over the

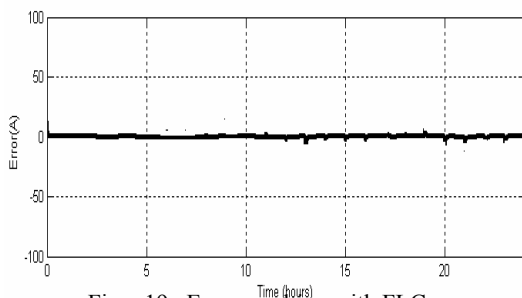simulation period

Fig.18 Error resulting with NNC

Figre 19   Error resulting with FLC

6. Conclusion

In this paper, a complete mathematical modeling and MATLAB simulink model for the different components of the PV-Wind hybrid system are developed and the system results are indicated a control system, which includes either the NNC or the FLC controller, is developed for coordinating the power flows among the different components of the PV-Wind hybrid system Simulation studies have been carried out to verify the PV-Wind hybrid system performance using an estimated electrical and load profiles and real weather data. The results show that the overall power management strategy is effective and the power flows among the different energy sources and the load demand is balanced successfully. The performance of the system is evaluated by comparing the performance of the system using the Neural Network Controller (NNC) and the Fuzzy Logic Controller (FLC). The response of output generation using FLC is more accurate and better than using NNC.

References

[1] Timur Gül, "Integrated Analysis of Hybrid Systems for Rural Electrification in Developing Countries", M.Sc.Thesis, Stockholm 2004.
 [2] Fukuda T, Shibata T. Theory and applications of neural networks for industrial control systems. IEEE IE 1992;39:472–89.
[3] Zurada JM, Marks RJ, Robinson CJ. Computational Intelligence Imitating Life. New York: IEEE Inc. Press, 1994.
[4] Y. Sukamongkol, S. Chungpaibulpatana, W.Ongsakul," A simulation model for predicting the performance of a solar photovoltaic system with alternating current loads", Renewable Energy, Vol.27,pp. 237–258, 2002.
[5] F. Lasnier and T.G .Ang , Photovoltaic Engineering Handbook, New York, 1990
[6] Mike Robinson, Paul Veers, Wind Turbine Control Workshop, Santa Clara University, Santa Clara, CA, June, 1997.
[7] S.A. Salle, D. Reardon, W.E. Leithead, M.J. Grimble, Review of wind turbine control, Int. J. Control
 Vol.52 ,pp.1295-1310, 1990.
[8] E. Muljadi, C.P. Butter"eld, P. Migliore, Variable speed operation of generators with rotor-speed feedback in wind power applications, Fifteenth ASME Wind Energy Symposium, Houston, Texas, 1996.
[9] SIMULINK. MathWorks, 3 Apple Hill Drive, Natick, MA 01760-2098, USA. URL: http:// www.mathworks.com.
[10] K. Ogata, Modern Control Engineering, Prentice-Hall Inc., Englewood Cliffs, N. J., 1990.
[11]. D. Driankov, H. Hellendoorn, and M. Reinfrank, An Introduction to Fuzzy Control, Springer-Verlag, Berlin, Heidelberg, 1993.